

Copyright © 1997, by the author(s).
All rights reserved.

Permission to make digital or hard copies of all or part of this work for personal or classroom use is granted without fee provided that copies are not made or distributed for profit or commercial advantage and that copies bear this notice and the full citation on the first page. To copy otherwise, to republish, to post on servers or to redistribute to lists, requires prior specific permission.

**MULTIFACTOR ELECTRON DISCHARGE PHYSICS
USING AN IMPROVED SECONDARY EMISSION
MODEL**

by

V. P. Gopinath, J. P. Verboncoeur, and C. K. Birdsall

Memorandum No. UCB/ERL M97/24

25 April 1997

**MULTIPACTOR ELECTRON DISCHARGE PHYSICS
USING AN IMPROVED SECONDARY EMISSION
MODEL**

by

V. P. Gopinath, J. P. Verboncoeur, and C. K. Birdsall

Memorandum No. UCB/ERL M97/24

25 April 1997

ELECTRONICS RESEARCH LABORATORY

College of Engineering
University of California, Berkeley
94720

Multipactor Electron Discharge Physics using an Improved Secondary Emission Model

V. P. Gopinath, J. P. Verboncoeur and C. K. Birdsall
Department of Electrical Engineering and Computer Sciences,
University of California
Berkeley, CA 94720

April 25, 1997

Abstract

This study details particle-in-cell simulations of the multipactor effect and discharges created using this effect. A detailed secondary emission model which accounts for the energy and impact angle dependence of yield is developed to simulate accurately the phenomenon. It is shown that a steady state multipactor can be built up from a very low density initial electron distribution and an oscillatory steady state can be achieved. The results for a more accurate secondary electron distribution are compared with simpler analytic models and extended. It is shown that, while the energy spread of secondary electrons differs from the monoenergetic analytical model, the weighted average energy is the same. Resistive loading of the circuit due to multipacting electrons is presented. The behavior of the system with Q values of between 20 and 200 is discussed.

1 Background

Multipactor effect is a resonant, low to medium voltage phenomenon and is frequently observed in electron beam devices, with RF or microwave driven cavities. Typically, the electrons hitting a surface with a maximum secondary emission ratio larger than unity, may avalanche to create more electrons. This avalanche happens when the phase of the driving RF voltage is such that the bunched electron beam always sees an accelerating field. The theory behind this phenomenon has been discussed in detail by several authors [1] – [6]. Vaughan [2] hypothesized that the avalanching stops when the inter-particle Coulomb force de-focuses the electron beam axially. It is also known that these electrons [2] can deposit considerable energies in a tiny spot resulting in significant surface damage and performance degradation. Therefore, it is important that multipactor evolution and the energy distribution of these electrons be well understood.

Kishek and Lau [3], [4] have developed analytical theory to study this phenomenon in terms of interaction of a few electron sheets with an external RLC circuit. In their study on multipactor-circuit interactions [3], they modeled the electron bunch as a single sheet (the density being a δ function) and analyzed its interaction with the external circuit. They numerically modeled the multipactor evolution to saturation and showed that the electron impact energy is equal to the lowest value that gives unity on the secondary electron yield curve (E_1 in Figure 1). They extended this study to a model containing two electron sheets [4] where they showed that the leading edge of the multipactor discharge grows at the expense of the trailing one and concluded that this would lead to tightly bunched electrons. They also presented the behavior of the system for different circuit Q values.

The current study extends their model by using a distribution of many electrons (sheets in 1d) which are initially uniformly loaded with a thermal electron velocity distribution. The simulation, done using a particle-in-cell (PIC) simulation code [10], is then allowed to evolve and a steady state multipactor or a decaying distribution, as the case may be, is obtained. In the current PIC simulations, the electrons and consequently, their densities are no longer constrained to be sharply peaked in space and are free to spread spatially depending on the circuit conditions.

In order to simulate this phenomenon accurately, a detailed secondary emission model is essential. The velocity distribution of the emitted secondaries is modeled carefully as described in Section 2. Sections 3 and 4 detail the PIC simulation and the results of simulations of multipactor phenomenon and comparison to the earlier simple analytic model.

2 Secondary Emission Model

A self-consistent secondary electron emission model is used in this study. The subsequent sections will discuss the impact on secondary emission and the properties of the emitted electrons due to the following:

- Dependence of number of secondaries emitted on the primary electron energy.
- Change in number of secondaries emitted due to angle of incidence of primary electron.
- Velocity distribution of the emitted secondaries (speed and angle).

2.1 Energy Dependence

Figure 1 shows a typical secondary electron yield vs. incident electron energy for a metal substrate (note: yield can change from > 1 for a smooth surface to < 1 for a rough one). It can be seen that the yield peaks at an incident energy of approximately 500 V and then decreases steadily after that. This peak is due to the fact that a relatively low energy incidence electron may not dislodge the secondary while a relatively higher energy primary will be in contact with surface atoms for too short a time [7]. It is also of interest to note the two points E_1 and E_2 on Figure 1, which are low and high energy points between which the yield of secondaries is greater than unity. In order to sustain a multipactor, the energy of the primary electrons should lie in this region. Vaughan [8] has modeled this curve analytically

$$\sigma = \sigma_{max}(we^{1-w})^k \quad (1)$$

where

$$w = \frac{(E_i - E_0)}{(E_{max} - E_0)} \quad (2)$$

and E_0 is the minimum threshold energy, E_{max} is energy at maximum yield and σ_{max} is the corresponding yield. k is a curve fit parameter given by

$$\begin{aligned} k &= k_1 = 0.62 \text{ if } w \leq 1 \\ k &= k_2 = 0.25 \text{ if } w > 1. \end{aligned} \quad (3)$$

Shih *et. al* [9] have conducted experiments on polished molybdenum and find that the above theory shows good agreement with their results.

2.2 Angular Dependence

The secondary yield normally increases with the incidence angle (0° signifies normal incidence). The theory of variation of yield with incidence is described in [7] and more recently in [8] and [9]. An analytical model of angular dependence is presented in Vaughan [8] which accounts for the variation of E_{max} and σ_{max} with energy and adds a “smoothness”

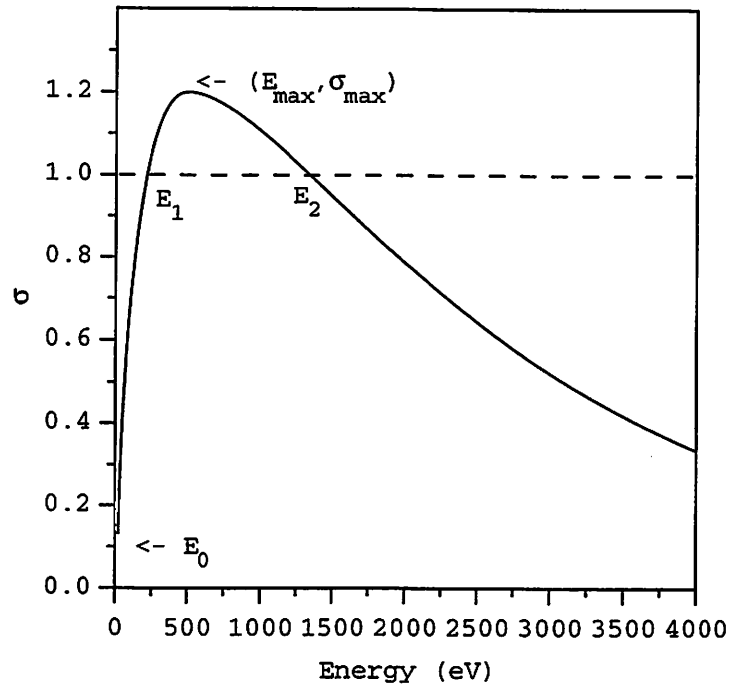


Figure 1: A Typical Metal Secondary Yield vs. Incidence Energy Curve [7].

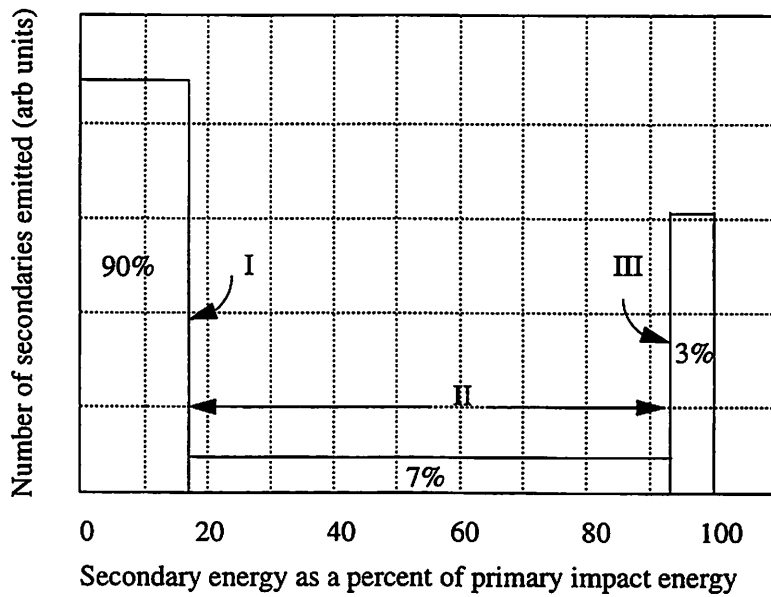


Figure 2: Relative energy distribution of secondary electrons, adapted from Spangenberg [7] fig. 4.17, pg 52), as used in the simulation.

parameter k_s in order to model the characteristic of the surface. This model modifies the values of σ_{max} and E_{max} as

$$\sigma_{max\theta} = \sigma_{max0}(1 + k_s\theta^2/\pi) \quad (4)$$

and

$$E_{max\theta} = E_{max0}(1 + k_s\theta^2/2\pi) \quad (5)$$

before using equations (1) and (2). The value of k_s lies between 0 (rough) and 2 (smooth).

2.3 Secondary Velocity Distribution

There are few references available regarding the velocity spread of the emitted secondaries. Spangenberg [7] mentions that secondary electrons are emitted with an isotropic angular velocity distribution irrespective of the incident electron velocity spread. The energy distribution of the emitted electrons, shown in Figure 2, includes:

- **Low Energy (I)** (true secondaries) 90% of the emitted electrons fall in this category with energies below 20 eV, peaking at around 10 eV. These are implemented in the simulation model by picking a random energy between 0-20 eV and then distributing them equally into the three velocity directions to provide an isotropic angular distribution.
- **Medium Energy (II)**: 7% of the emitted particles lie in this energy range with energies ranging from 20 eV to 98% of the incident electron energy. The velocity distribution in the simulation is calculated the same way as in the low energy case.
- **High Energy (III)**: (reflected primaries) These are not really secondary electrons but reflected primaries. 3% of the secondaries lie in this energy range which peaks around 99% of the incident electron energy. The reflected primary is emitted specularly, i.e. the angle of reflection is equal to the angle of incidence. This is achieved by inverting the sign of v_x and keeping the signs of v_y and v_z the same.

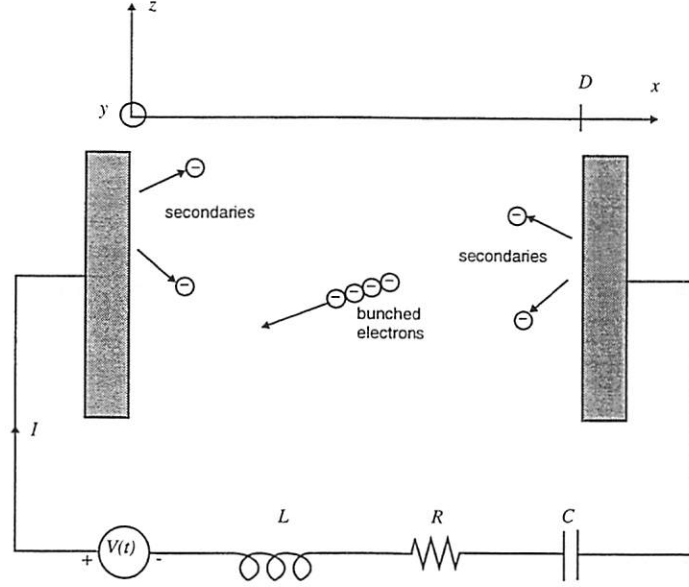


Figure 3: Simulation Model, $R=20\ \Omega$, $L=32.48\ \text{nH}$, $C=1$, $f_{RF} = 2.45\text{GHz}$, $V_{RF} = 13.333\ \text{V}$, $A = 1.337 \times 10^{-5}\text{m}^2$ and $D = 9.1 \times 10^{-4}$.

3 Simulation Details

The particle-in-cell code XPDP1 [10] was used to simulate a 1d3v parallel plate discharge. The model consists of an RF source with series RLC components as shown in Figure 3. The results of the simulation shown is for the case where the RF drive is, $f_{RF} = 2.45\ \text{GHz}$, $V_{RF} = 13.33\ \text{V}$. The external circuit has $R = 20\ \Omega$, $L = 32.48\ \text{nH}$, resulting in a circuit Q of 25. This is similar to that used in Kishek and Lau [3] and is meant to model a cavity or gap in, say, a klystron. Their work used a parallel current driven RLC circuit and this study uses its Norton equivalent, a voltage driven series RLC circuit [5] shown in Figure 3. The external capacitance is set to a very large value to act as a short circuit. The parallel plate system is now designed so that under vacuum conditions, the external inductance and the parallel plate capacitance are in resonance ($\omega_{RF} = 1/\sqrt{L_{ext}C_{gap}}$). This leads to cavity dimensions of length $D = 9.1 \times 10^{-4}\ \text{m}$ and area $A = 1.337 \times 10^{-5}\ \text{m}^2$. The resulting voltage drop across the vacuum gap is 333 V and is compensated by an equal and out-of-phase drop across the external inductor. The wall is assumed to be made of copper with $\sigma_{max} = 1.2$, $E_{max} = 400.0\ \text{eV}$ with a corresponding $E_1 = 175\ \text{eV}$ and $E_2 = 1500\ \text{eV}$, as shown in Figure 1. It should be noted here that the wall was assumed to have a non-zero emission threshold, E_0 , of 15 eV.

For the low Q (< 50) cases, the system is started with a uniformly (spatially) loaded low density Maxwellian (3v) distribution of velocities. Within a few RF cycles, most of the out of phase electrons are lost to the walls. A high Q circuit takes relatively longer

time to ring up to the steady state voltage. Loading such a system with a low density initial distribution results in the loss of all the electrons to the wall without creating any secondaries since the wall potential takes a long time to raise above E_1/q . This problem was resolved by emitting a one time, low current density beam after $2L/R$ seconds over one RF cycle. In reality, there is a constant source of cosmic rays that generate a steady low density electron density background. The electron “seed” is allowed to evolve and a small bunch of in-phase electrons “see” an accelerating electric field and begin to avalanche. Eventually, the space charge forces modify the phase of the bunched beam vis-a-vis the external drive, to bring the system to a steady state. The unloaded Q of the series circuit, given by $\omega L/R$, is equal to 20 for the base run. The simulation code treats the external circuit self consistently [11] and hence is capable of resolving the time evolution of the gap voltage correctly for the different Q cases.

In order to study the behavior of the system with respect to the circuit Q , runs were done with the external resistance between 500Ω and 25Ω resulting in Q values between 20 and 200 respectively. The voltage of the driving RF signal is changed accordingly so the potential across the unloaded gap, given by $V_{RF}X_C/R$, where X_C is the impedance of the gap, is the same for all cases. The other circuit parameters are held unchanged.

4 Simulation Results

The analysis by Kishek and Lau [4] assumed that the emitted secondaries were created with zero drift velocity. In order to verify the model used in this study and to verify their analytic results, a few simulations were run with many particles. The PIC simulation approximated this by creating all secondaries cold with a small initial drift of 1 eV.

The first subsection details our simulation results obtained for their model, finding agreement. The second subsection shows the results for the cases with the distributed secondary emission model included.

4.1 Mono-energetic emission case

This study was done to compare the simulation with available analytical theory of Kishek and Lau ([3], [4]). The created secondary electrons were all given an initial energy of 1 eV. It was noticed that the electron beam in this simulation run was tightly bunched, similar to the one-sheet analytic model, (as was expected) and the simulation, relative to the distributed emission case discussed later, reached equilibrium sooner. The electron energy distribution of the particles hitting the wall was also seen to be sharply peaked around 182 eV as shown by the dotted line in Figure 4. Calculating the weighted average of the distribution function $\Sigma Ef(E)/\Sigma f(E)$ results in a value of 175.83 V which is exactly equal to the value of E_1 for this simulation run and matches the analytical prediction accurately. Further, as predicted in [4], the electrons were tightly bunched in space.

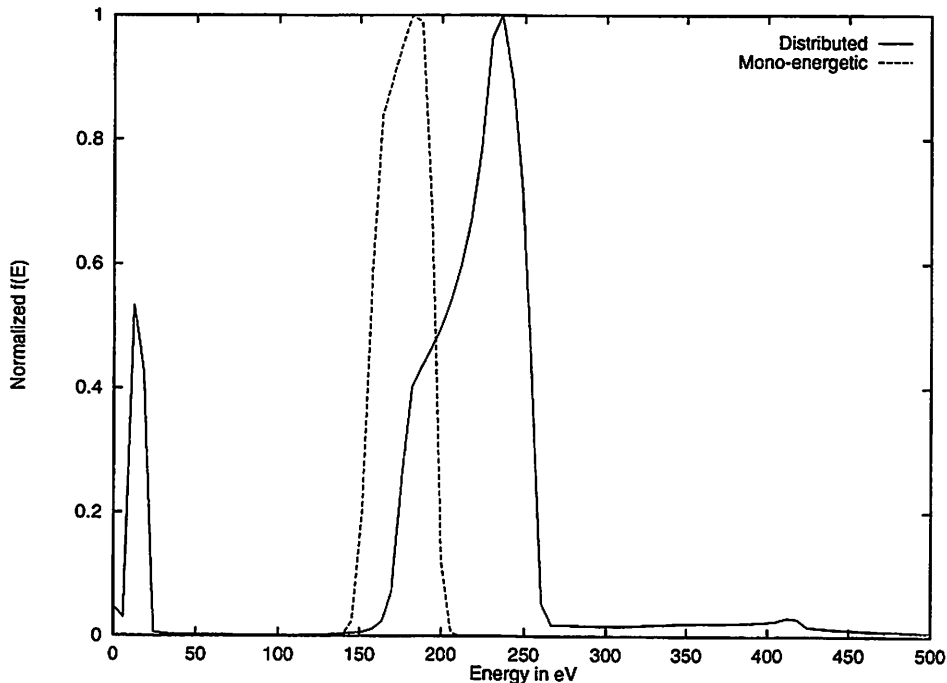


Figure 4: Comparison between the mono-energetic emission model with the distributed emission model

4.2 Detailed Emission Case

This section discusses the results of simulations run using the full thermal secondary emission model described in Section 2. The energy distribution of the electrons hitting the wall is shown as the solid line in Figure 4. It can be seen that the results are different (shifted) for the simple mono-energetic emission case. The maximum energy of the electrons is now approximately 237 eV. In addition there is a substantial number of electrons hitting the wall at much lower energies. Further, there is a small number of high energy electrons corresponding to the reflected primaries. The weighted average energy for the distributed model is 215 eV. In order to estimate accurately the average energy of the electrons hitting the wall, the effect of non-zero initial emission energy has to be accounted for. This can be done by simply averaging over the emission distribution function, shown in Figure 2 and described in Section 2.3 and is given approximately as $(0.9 * E_0 + 0.07 * E_{\max}/2 + 0.03 * E_{\max})$ giving a value of 39 eV. Subtracting this value from the weighted average gives a value of 175.5 eV which is again close to E_1 .

The time evolution of the number of electrons in the multipactor is shown in Figure 5. It can be seen that the number initially drops from 1.1×10^4 almost to zero, indicating the loss of out-of-phase particles and then rapidly rises due to multipacting, eventually reaching an oscillating steady state. The inset shows particle number over a few cycles in steady

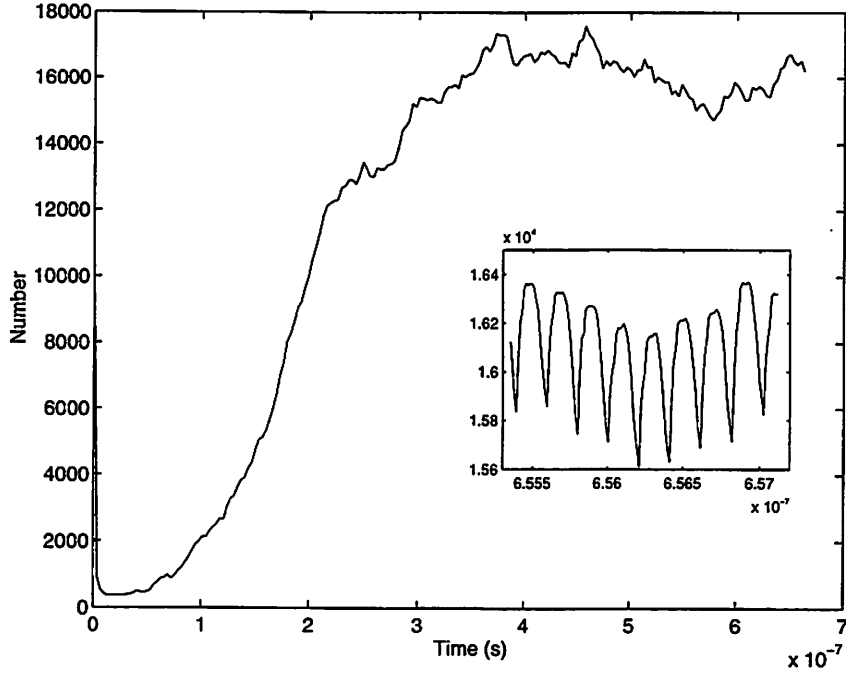


Figure 5: Time evolution of electrons

state.

The relation between the driving voltage and particle number (and hence its phase) through the system can be seen in Figure 6. The effect of the phase of the driving voltage on the particle number can be seen with an oscillating steady state, with the number of particles holding steady during about a transit time. The period of the driving voltage is equal to two transit times of the electron bunch in steady state.

Figures 7-a and 7-b shows a snapshot of velocity phase space of the electrons and the corresponding density, respectively. A bunch of electrons is moving to the left in the $-x$ direction. In addition, there is a smaller set of electrons that have already hit the left wall and are creating secondaries; this set is the reflected primaries from the right wall with velocities greater than the main bunch. The secondaries created by this set are out of phase with the driving voltage and will be absorbed.

The effect of the multipactor electrons on the steady state circuit characteristics can be seen in terms of resistive loading of the steady gap state voltage. The vacuum steady state peak gap voltage is 333.33 Volts for all the Q cases discussed earlier. However, the loaded steady state voltage is seen to be lower for all cases, indicating resistive loading due to beam electrons. The change in the phase angle of the cavity impedance is quite small, being no larger than $\tan^{-1}(1/200) = 0.2864^\circ$ for the worst case. Therefore, the reduction in voltage is due to the resistive loading of the gap by the beam. The value of the equivalent resistance can be calculated by dividing the driving voltage by the steady state current and

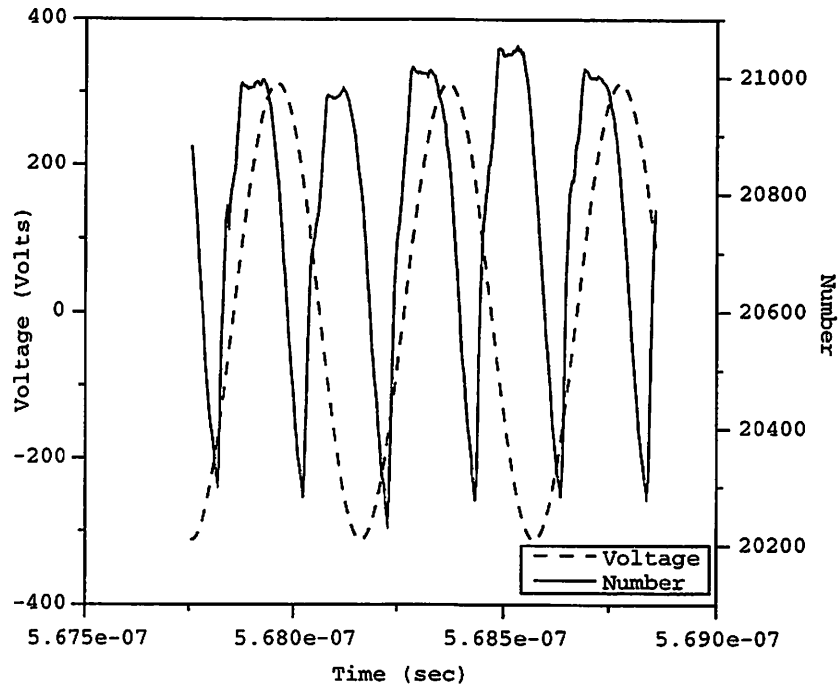


Figure 6: Plot of gap voltage and number of particles vs. time.

these values are listed in Table 1. This resistance is used to calculate the power dissipation due to the beam and the results are shown on the right axis of Figure 8. The same figure plots the steady state electron number in the gap vs. Q . As expected, the lower Q systems show higher resistive loading and can sustain a higher steady state electron density. The average steady state number of electrons in the system, plotted on the left axis of Figure 8, increases from ≈ 1034 for $Q = 200$ to ≈ 6900 for $Q = 20$.

Table 1: Resistance at Different Q .

Q	Resistance Ω
20	1.516
25	1.273
50	0.788
100	0.301
200	0.082

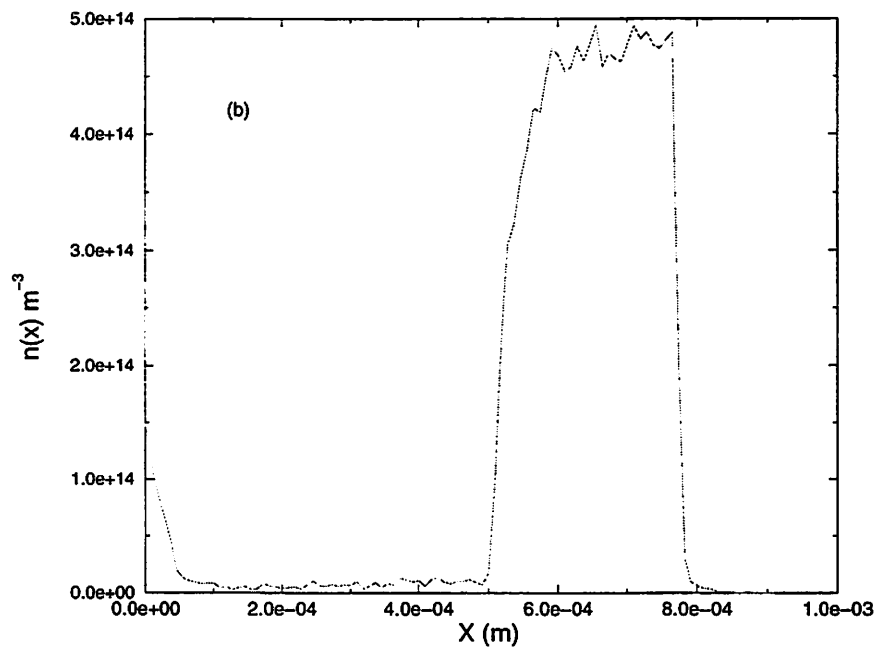
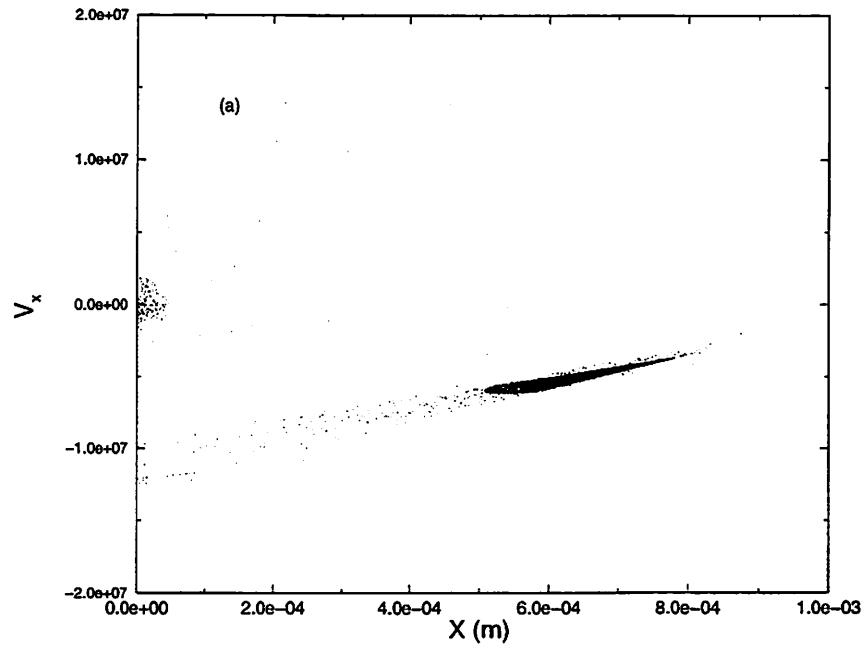


Figure 7: (a) Instantaneous velocity phase space and (b) number density corresponding to above.

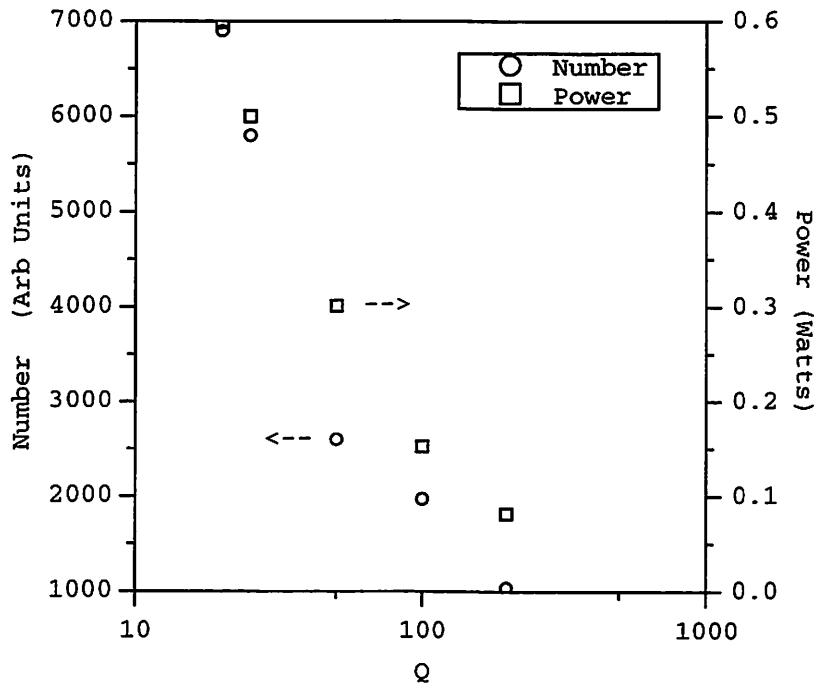


Figure 8: Variation of resistive loading and steady state electron number with circuit Q

5 Conclusions

Simulations of electron multipactor discharges have been presented. Many particle simulations agree with earlier analytic theory when the secondary electrons are emitted mono-energetically. The analytic results differ with the simulation for the full range of secondary emission case. However, the weighted average energy of the emitted electrons at steady state is still, as predicted from theory, close to E_1 . The effect of the Q on steady state multipactor characteristics are explained in terms of resistive loading by the electron beam. Lower Q cavities are shown to sustain higher density electron beam, and consequently, higher resistive beam loading.

6 Acknowledgments

We thank Rami Kishek for discussions and help in setting up an initial RLC circuit. Thanks are due to Y. Y. Lau, D. Chernin and A. Shih for discussions on details of secondary emission. Thanks are also due to Peggy Christenson for the pointers on beam loading. This work was supported in part by the Office of Naval Research under Contract FD-N00014-90-J-1198 and AFOSR under grant F49620-92-J0487.

References

- [1] A. H. W. Beck, *Space-Charge Waves and Slow Electromagnetic Waves*, pp. 211, Pergamon Press, 1958.
- [2] J. R. M. Vaughan, *IEEE Trans. ED-35*, 1172 (1988).
- [3] R. A. Kishek and Y. Y. Lau, "Interaction of Multipactor Discharge and RF Circuit," *Phys. Rev. Lett.* Vol. 75, No 6, Aug. 1995.
- [4] R. A. Kishek and Y. Y. Lau, "A novel phase focusing mechanism in multipactor discharge," *Phys Plas.* 3 (5), May 1996.
- [5] Rami. A. Kishek, Personal Communications on setting up initial circuit parameters for PIC simulation.
- [6] S. Riyopolous, D. Chernin and D. Dialetis, "Theory of Electron Multipactor in crossed-fields," *Phys Plas.* 2 (8), Aug 1995.
- [7] Karl R. Spangenberg, *Vacuum Tubes*, McGraw-Hill, New York, 1948, pp. 48–57.
- [8] J. R. M. Vaughan, "A New Formula for Secondary Emission Yield," *IEEE Trans. ED-36*, 1963 (1989).
- [9] A. Shih and C. Hor, "Secondary Emission Properties as a Function of the Electron Incidence Angle" *IEEE Trans. ED-40*, 824 (1993).
- [10] J. P. Verboncoeur, V. Vahedi, M. V. Alves and C. K. Birdsall, *PDP1, PDC1 and PDS1: Plasma Device one-dimensional Bounded Electrostatic Codes*, Plasma Theory and Simulation Group, University of California, Berkeley, CA 94720. Available via <http://ptsg.eecs.berkeley.edu>.
- [11] J. P. Verboncoeur et. al., "Simultaneous Potential and Circuit Solution for 1D Bounded Plasma Particle Simulation Codes," *J. Comp. Phys.*, Vol. 104, No. 2, Feb. 1993.